Dynamic spin fluctuations in the frustrated spin chain compound $Li_3Cu_2SbO_6$

A. Bhattacharyya [1,*] T. K. Bhowmik,[2] D. T. Adroja,[3,4,†] B. Rahaman,[5] S. Kar,[6] S. Das,[7] T. Saha-Dasgupta,[7,‡] P. K. Biswas,[3] T. P. Sinha,[2] R. A. Ewings,[3] D. D. Khalyavin,[3] and A. M. Strydom[4,8]

[1]*Department of Physics, Ramakrishna Mission Vivekananda Educational and Research Institute, Belur Math, Howrah 711202, West Bengal, India*

[2]*Department of Physics, Bose Institute, 93/1, Acharya Prafulla Chandra Road, Kolkata 700009, India*

[3]*ISIS Facility, Rutherford Appleton Laboratory, Chilton, Didcot Oxon, OX11 0QX, United Kingdom*

[4]*Highly Correlated Matter Research Group, Physics Department, University of Johannesburg, PO Box 524, Auckland Park 2006, South Africa*

[5]*Department of Physics, Aliah University, Newtown, Kolkata 700156, India*

[6]*Department of Physics, A.K.P.C. Mahavidyalaya, Hooghly 712611, India*

[7]*S.N. Bose National Centre for Basic Sciences, Salt Lake, Kolkata 700106, India*

[8]*Max Planck Institute for Chemical Physics of Solids, Nothnitzerstrasse 40, D-01187 Dresden, Germany*

(Received 3 March 2021; revised 30 April 2021; accepted 3 May 2021; published 20 May 2021)

We report the signatures of dynamic spin fluctuations in the layered honeycomb $Li_3Cu_2SbO_6$ compound, with a $3d$ $S = 1/2$ d^9 Cu^{2+} configuration, through muon spin rotation and relaxation (μSR) and neutron scattering studies. Our zero-field (ZF) and longitudinal-field (LF) μSR results demonstrate the slowing down of the Cu^{2+} spin fluctuations below 4.0 K. The saturation of the ZF relaxation rate at low temperature, together with its weak dependence on the longitudinal field between 0 and 3.2 kG, indicates the presence of dynamic spin fluctuations persisting even at 80 mK without static order. Neutron scattering study reveals the gapped magnetic excitations with three modes at 7.7, 13.5, and 33 meV. Our density functional theory calculations reveal that the next-nearest-neighbor (NNN) antiferromagnetic (AFM) exchange ($J_{AFM} = 31$ meV) is stronger than the NN ferromagnetic (FM) exchange ($J_{FM} = -21$ meV), indicating the importance of the orbital degrees of freedom. Our results suggest that the physics of $Li_3Cu_2SbO_6$ can be explained by an alternating AFM chain rather than the honeycomb lattice.

DOI: 10.1103/PhysRevB.103.174423

Low-dimensional honeycomb layered oxide materials that consist of alkali-metal atoms sandwiched between slabs of transition metal and chalcogen or pnictogen atoms arranged in a honeycomb fashion are of great interest at present because these materials play host to fascinating symmetry-protected topological phases, and they are crucial for next-generation cathode materials for rechargeable batteries [1]. The emergent properties that they exhibit are the Haldane gap, fractionalization of spin degrees of freedom, and a topological quantum spin liquid (QSL) state with exotic quasiparticles for a honeycomb lattice in which the spins fractionalize into emergent quasiparticle-Majorana fermions [2–7]. Experimental progress has been achieved in QSL states in realistic materials, including organic anisotropic triangular-lattice Mott insulators [κ-$(ET)_2Cu_2(CN)_3$ [8] and $EtMe_3Sb[Pd(dmit)_2]_2$] [9], the kagome-lattice system [$ZnCu_3(OH)_6Cl_2$] [10], and the three-dimensional hyperkagome-lattice system $Na_4Ir_3O_8$ [11]. Despite the large magnetic exchange $J \approx 250$ K observed in these systems [8–11], there is no experimental indication of long-range magnetic ordering down to a temperature of ~30 mK. Candidate materials for QSL are $5d$ and $4d$ transition metal compounds with the d^5-electron configuration, such as iridates α-Na_2IrO_3, α-Li_2IrO_3, $H_3LiIr_2O_6$, $Ag_3LiIr_2O_6$, and ruthenium-based α-$RuCl_3$ [12–16]. Iridate materials crystallize in an alternating two-dimensional (2D) layered structure in which IrO_6 octahedra form a honeycomb network by sharing the three orthogonal edges of an octahedron with 90° Ir-O-Ir bonds. The orthogonal anisotropies of the three nearest-neighbor bonds of each spin conflict with each other, leading to frustration. A QSL state has been seen for $H_3LiIr_2O_6$, while other candidates of $LiIr_2$ type were magnetically ordered due to Heisenberg interactions caused by d-d exchange coupling, which compete with Kitaev-type interactions, and supporting a magnetically ordered state [16].

In the case of the $3d$ d^7 quasi-2D honeycomb lattice $A_3A'_2BO_6$ (A = Li, Na; A' = Co, Ni; B = Sb, Te) depending upon the anisotropy and frustration triggered by the competition between antiferromagnetic (AFM) and ferromagnetic (FM) exchange interactions, numerous forms of unusual ordering are found such as FM, AFM, zigzag AFM, and stripe order AFM, which is anticipated to have the same origin as in the d^{5+} materials, that is, due to Kitaev-type interactions [17–20]. Turning to the title material of this paper, the d^9 $Li_3Cu_2SbO_6$ compound crystallizes in a distorted honeycomb lattice with edge-sharing CuO_6 octahedra with space group $C2/m$ [21]. The bond geometry of the Cu-O-Cu bond

*amitava.bhattacharyya@rkmvu.ac.in
†devashibhai.adroja@stfc.ac.uk
‡tanusri@bose.res.in

angle resembling ≈90° puts this material close to a QSL-like state [21,22]. The frustration index is defined as $f = |\theta/T_{N,f}|$, where θ is the Weiss temperature and $T_{N,f}$ is either the Néel temperature or the spin freezing temperature. The lack of a magnetic transition down to 50 mK in $Li_3Cu_2SbO_6$ indicates that it is highly frustrated. Here we present the ground-state spin dynamics of $Li_3Cu_2SbO_6$ through a muon spin relaxation study. Notably, below ∼4.0 K, a novel and unusual spin state appears, which does not reveal any magnetic ordering down to 50 mK. Neither the oscillations in the time-dependent asymmetry nor the 2/3 drop in the initial asymmetry are observed in the zero-field (ZF) spectra down to 80 mK, confirming the absence of long-range ordering. The absence of magnetic peaks is confirmed by neutron diffraction data at 50 mK, thus ruling out any long-range magnetic ordering. The muon spin relaxation rate measured in ZF exhibits a plateau below 1.0 K. These observations suggest that a QSL-like ground state is formed in $Li_3Cu_2SbO_6$. Furthermore, our inelastic neutron study reveals the presence of gapped magnetic excitations at 7 K, which can be explained using the exchange parameters estimated from our density functional theory (DFT) calculation.

I. SAMPLE PREPARATION AND CHARACTERIZATION

A single-phase polycrystalline $Li_3Cu_2SbO_6$ sample was prepared employing a solid-state reaction method. Li_2CO_3 (BDH, 99%), Sb_2O_3 (Aldrich, 99.99%), and CuO (Cerac, 99.999%) powder was thoroughly ground and pressed into a pellet. The pellet was placed in an alumina boat and heated to 900 °C. It was cooled down to 600 °C in 100 h in air finally, the furnace was turned off. Magnetization measurements were performed using superconducting MPMS-XL7AC. The specific heat was measured using PPMS with a ^{3}He / ^{4}He dilution refrigerator. High-resolution neutron powder diffraction, μSR and inelastic neutron scattering data were collected at the ISIS Pulsed Neutron and Muon Source of Rutherford Appleton Laboratory, U.K.

II. CRYSTAL STRUCTURE AND THERMODYNAMICS PROPERTIES

The crystal structure was refined by the Rietveld method using neutron diffraction (ND) data collected at 50 mK and 10 K, as presented in Figs. 1(a) and 1(b) of the supplemental material (SM) [23]. There is no difference between these two ND spectra. No new peaks are detected down to 50 mK, which is about four orders of magnitude lower than the J_{AFM} value of 31 meV (359 K), indicating the absence of long-range magnetic ordering. The distorted honeycomb phase was indexed, which crystallizes in the monoclinic space group $C2/m$ as shown in Figs. 1(a)–1(c), isostructural with other compounds in this series [19,24,25]. The $\chi(T)$ data as shown in Fig. 2(a) of the SM do not show any feature of long-range magnetic order down to 1.8 K in agreement with ND data. The linearity of inverse $\chi(T)$ data at high $T > 200$ K (I) and low $T < 30$ K (II) temperatures suggest two different regions of Curie-Weiss (CW) -like behavior. The analysis yields that the number of $S = 1/2$ Cu^{2+} spins effective at high T is about 1.0/f.u. The difference of $\chi^{exp} - \chi^{CW}$

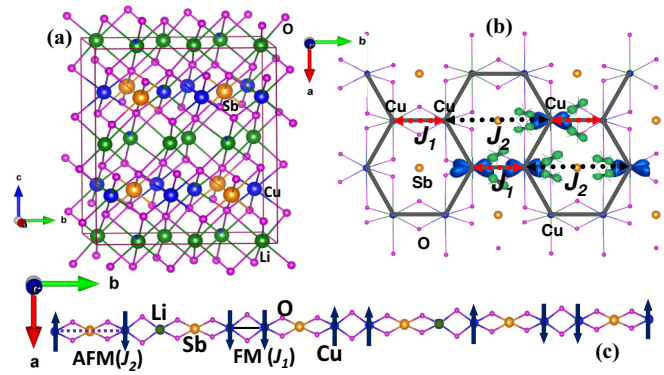

FIG. 1. (a) The monoclinic unit cell representation of $Li_3Cu_2SbO_6$. (b) Sketch of the *ab*-plane of the $Li_3Cu_2SbO_6$ honeycomb structure (the gray hexagon illustrates the underlying honeycomb structure). The Cu-O bond length and Cu-O-Cu bond angles are given in figure. (c) The FM-AFM chain is formed by Cu ions along the *b*-axis in the *ab*-plane, whereas the Li-ion acts as the nonmagnetic defect and produces the fragmented Cu-spin chains.

presented in the inset of Fig. 2(a) of the SM, shows thermally activated behavior. The peak appears near 80 K. The $\chi(T)$ data well accounted with our calculated FM-AFM exchange interactions with $J_{FM} = -21$ meV and $J_{AFM} = 31$ meV (see DFT calculation). The absence of a λ-type anomaly in heat capacity data rules out the possibility of any long-range ordering, which supports the susceptibility and neutron diffraction data as shown in Fig. 2(b) of the SM. A Schottky-like feature in the heat capacity is observed around ≈2 K, as shown in the inset of Fig. 2(b) of the SM. Similar anomalies observed

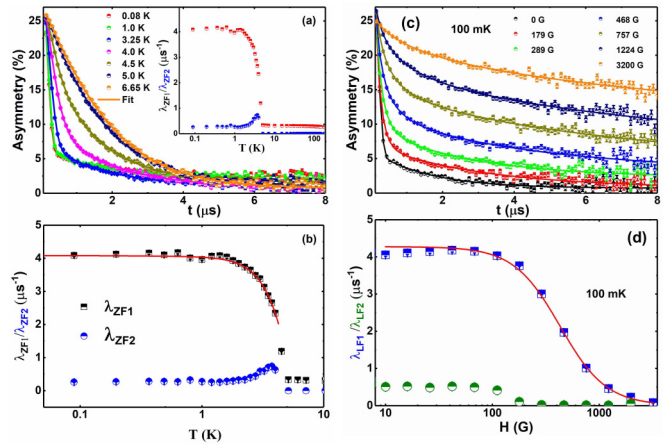

FIG. 2. (a) Time-dependent muon spin polarization of $Li_3Cu_2SbO_6$ at selected temperatures measured in zero field. Solid lines are fits to the data (see text), which consists of two relaxation processes, λ_{ZF_1} and λ_{ZF_2}, which are the fast and slow relaxation rates, respectively. The two relaxation processes were found to have a weighting ratio 5:1. This is consistent with the ratio of the two muon sites expected from the crystal structure. (b) Temperature dependence of λ_{ZF_1} and λ_{ZF_2}. (c) Time-dependent muon spin polarization of $Li_3Cu_2SbO_6$ at selected longitudinal applied fields at 100 mK. Solid lines are fits to the data (see text). (d) LF dependence of the muon spin relaxation rate at 100 mK. The line represents the fit to the data (see text).

in herbertsmithite $KCu_6AlBiO_4(SO_4)_5Cl$, this behavior was attributed to short-range spin correlations on the interlayer sites [26,27]. It is interesting to note that the magnetic entropy reaches a value of $0.5R\ln 2$ near 16 K, suggesting short-range ordering [Fig. 2(c) of the SM].

III. ZF-μSR: EVIDENCE FOR SHORT-RANGE CORRELATIONS

No indication of long-range magnetic ordering has been found down to 50 mK through neutron diffraction, magnetic susceptibility, or specific-heat measurements, which motivated us to measure the zero-field (ZF) and longitudinal-field (LF) muon spin relaxation (μSR) of $Li_3Cu_2SbO_6$ down to 80 mK. ZF/LF-μSR is an exceptional tool to probe static and dynamic magnetic fluctuations or quantum magnetism, and it is often employed to unravel the enigmatic QSL state. Figure 2(a) represents the ZF-μSR data at different temperatures, which consist of the local responses of muons embedded at various stopping sites of $Li_3Cu_2SbO_6$. Our important observations from the ZF-μSR data are (a) the lack of oscillations in muon spectra, as it usually seen for magnetically ordered systems, and (b) no loss of the initial asymmetry at time $t = 0$ down to 80 mK. These observations strongly suggest the absence of static magnetism in $Li_3Cu_2SbO_6$, and they signify a slowing down of the spin dynamics. We have used several relaxation functions to fit our ZF and LF-μSR data, starting from (a) simple exponential decay, (b) stretched exponential, and (c) Umerao spin-glass. The best fit is obtained using a stretched exponential relaxation plus a decaying exponential function with a constant background term, $G_z(t) = A_1 \exp[-(\lambda_{ZF_1} t)^{\beta_{ZF}}] + A_2 \exp(-\lambda_{ZF_2} t) + A_{bg}$, where the first two terms reflect the contribution of the muons that stop within the sample, and the third term accounts for those muons that stop within the sample holder. The slow and fast exponential decays λ_{ZF_1} and λ_{ZF_2}, respectively, represent a two-component electronic spin contribution to the muon depolarization. $A_1 \sim 21\%$ and $A_2 \sim 4\%$ are the initial asymmetry values, $\lambda_{ZF_1}/\lambda_{ZF_2}$ are the muon spin relaxation rate, and β_{ZF} is the stretching exponent. This approach has also been used in the analysis of the QSL-like candidates $SrCr_2Ga_8O_{19}$ [28] and $Sr_2Cu(Te_{0.5}W_{0.5})O_6$ [29]. The coefficient $A_{bg} \sim 0.5\%$ is a background constant representing muons that missed the sample. The solid curves show the fits of ZF-μSR data in Fig. 2(a). Figure 2(b) shows the temperature dependence of the spin depolarization rate, λ_{ZF_1}, λ_{ZF_2}, and the stretching component, β_{ZF} [Figs. 3(a) and 3(b) of the SM, respectively].

The important result shown in Fig. 2(b) is that there is no static magnetism in $Li_3Cu_2SbO_6$ upon cooling to at least 80 mK, which agrees with the neutron diffraction, susceptibility, and heat capacity data as presented above. Therefore, the magnetic fluctuations remain dynamic down to the lowest temperature of measurements, an indispensable criterion for a system to undergo any transition to a spin freezing state. The rise of λ_{ZF_1} below 4 K designates the slowing down of Cu^{2+} spin fluctuations as a consequence of short-range interactions. It is interesting to note that below 1 K, the λ_{ZF} shows a temperature-independent plateaulike behavior [see Fig. 2(b)], which signifies the presence of dynamic spin fluctuations. The

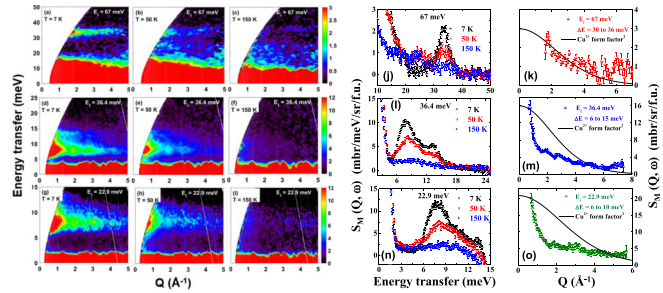

FIG. 3. Left panels (a)–(i) show the estimated magnetic scattering of $Li_3Cu_2SbO_6$ at 7, 50, and 150 K obtained after subtracting phonon scattering. Panels (a)–(c) are for $E_i = 67$ meV, (d)–(f) are for $E_i = 36.4$ meV, and (g)–(i) are for $E_i = 22.9$ meV. The strong scattering near zero energy transfer is mainly due to the incoherent background and elastic scattering. Right panels (j)–(o) show the scattering angle integrated ($2\theta = 8°$–$35°$) 1D-energy cuts of the magnetic intensity, from the color maps, plotted as intensity vs energy transfer at 7, 50, and 150 K, (j) for $E_i = 67$ meV, (l) for $E_i = 36.4$ meV, and (n) for $E_i = 22.9$ meV. Note that the slightly negative signal at larger energy transfer, especially in 22.9 meV, is an artifact of the phonon background subtraction due to frame-overlap in multi-E_i measurements. Right panels (k),(m),(o) show the energy integrated momentum-dependent (Q) magnetic intensity of three magnetic excitations at 7 K. The solid line shows the normalized magnetic form-factor squares [$F^2(Q)$] of the Cu^{2+} ion.

plateaulike behavior in λ_{ZF} versus T data has also been seen in other QSL candidates [30,31]. The stretching exponent β_{ZF} [Fig. 3(a) of the SM] approaches 1 near 2 K, which suggests fast fluctuating local internal fields. Below 2 K, β_{ZF} increases with decreasing temperature and attains a maximum value of $\sim$2 at 80 mK, suggesting Gaussian field distributions produced by magnetic exchange interactions of nearest-neighbor spins. This type of behavior of β_{ZF} designates the slowing down of magnetic fluctuations at low temperatures. Similar β_{ZF} values are observed in the QSL candidates $SrCr_2Ga_8O_{19}$ [28] and $Sr_2Cu(Te_{0.5}W_{0.5})O_6$ [29].

IV. LF-μSR: PROBING THE SPIN-SPIN CORRELATIONS

To understand the nature of dynamic spin fluctuations, we further examine the LF-μSR data at different fields from 1 mT up to 320 mT measured at 100 mK, as shown in Fig. 2(c). The size of the internal field distributions is estimated as $\Delta = 1$ mT, where $\gamma_\mu = 135.5 \times 2\pi$ s^{-1} μT^{-1} is the gyromagnetic ratio for muons. The absence of saturation of LF-μSR spectra at 320 mT infers that the plateaulike behavior is not associated with static magnetic fluctuations, as seen for magnetically ordered systems. Hence it must be linked with dynamic fluctuations as observed for QSL-like systems [32]. The field dependence of λ_{LF} is shown in Fig. 2(d); the observed plateaulike behavior suggests the slowing down of spin fluctuations. This could be associated with spin-liquid-like behavior similar to μSR observations reported for $Ce_2Sn_2O_7$ [33] and $SrDy_2O_4$ [34]. We have fitted $\lambda_{LF}(H)$ using Redfield's equation, $\lambda_{LF} = \lambda_{LF_0} + \frac{2\gamma_\mu^2 \Delta^2 \tau_C}{1+\gamma_\mu^2 H^2 \tau_C^2}$, where Δ represents the amplitude of the internal field distribution, and the relaxation timescale of spin fluctuations is τ_C. The fit to the

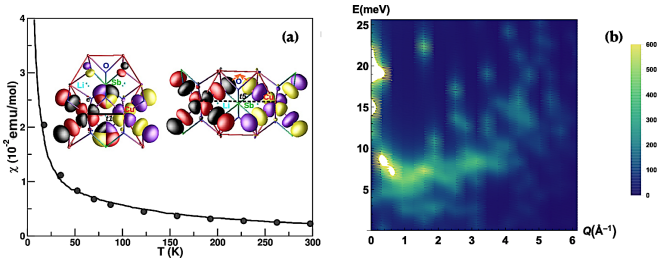

FIG. 4. (a) Calculated spin susceptibility (circles) of the fragmented FM-AFM $S = 1/2$ chain model of the $Li_3Cu_2SbO_6$ compound in comparison to the experimental data. The inset shows the plot of effective Cu x^2-y^2 Wannier functions placed at two neighboring Cu sites connected by t_1 hopping (left) and t_5 hopping (right). See text for details. (b) The calculated dynamical structure factor using the exact diagonalization (ED) method.

$\lambda_{LF}(H)$ data is given by the solid red line in Fig. 2(d). The calculated parameters are $\lambda_{LF}(0) = 0.003\ \mu s^{-1}$, $\Delta = 1$ mT, and $\tau_C = 2.7 \times 10^{-8}$ s.

V. INELASTIC NEUTRON SCATTERING: MAGNETIC EXCITATIONS

The results of INS study for incident energies $E_i = 67$, 36.4, and 22.9 meV are presented in Figs. 3(a)–3(i) as color maps of the scattering intensity, and energy transfer versus momentum transfer (Q) at 7, 50, and 150 K. The data have been corrected with phonon scattering using the measured data at 300 K and using the Bose factor. Further, the one-dimensional scattering angle-integrated (or Q-integrated) energy cuts from the color intensity maps at the lower scattering angles [where the magnetic scattering is dominated as it follows the magnetic form-factor squares, $F^2(Q)$, of the Cu^{2+} ion], and the higher scattering angles [where the phonon scattering is dominated as the phonon scattering increases as Q^2], are plotted in Fig. 4 of the SM. Figures 3(a), 3(d), and 3(g) show that at 7 K, we have three magnetic excitations near 33, 13.5, and 7.7 meV. With the increasing temperature at 50 K, the intensity of all three excitations decreases (see Fig. 3). It is interesting to note that at 50 K, no apparent change in the phonon intensity at high angles (see Fig. 4 of the SM) has been seen compared with 7 K in 67 meV data. In comparison, at a low angle, a weak increase in the intensity near 25 meV has been observed at 50 K compared to 7 K. Further, at 150 K, the intensity of all three modes (7.7, 13.5, and 33 meV) is reduced considerably. Upon closer inspection, the color plots of 150 K in Fig. 3 indicate that scattering has moved to lower Q and lower energy at 150 K, which might suggest that ferromagnetic-like short-range correlations exist in the high-temperature range. This has also been supported by the data of 36.4 and 22.9 meV at 150 K. To check whether the energy of three observed magnetic excitations exhibits any dispersion (i.e., Q dependence) at 5 K, we made 1D cuts at various Q-positions (not shown here) and found that the energy of all the magnetic excitations is nearly Q-independent.

VI. THEORETICAL CALCULATIONS

To achieve a theoretical understanding of the electronic and magnetic behavior of $Li_3Cu_2SbO_6$, we have carried out first-principles density functional theory (DFT) calculations [35], and we obtained a solution of the DFT-derived spin Hamiltonian by quantum Monte Carlo and exact diagonalization. The non-spin-polarized band structure, assuming a perfectly ordered compound with no intermixing between Li and Cu sites, shows two Cu x^2-y^2 bands at the Fermi level strongly admixed with O p and Sb states, corresponding to two Cu^{2+}, d^9 ions in the monoclinic $C2/m$ unit cell. The magnetic moments at Cu, O, and Sb in a spin-polarized calculation turned out to be $0.49\mu_B$, $0.09\mu_B$, and $0.02\mu_B$, respectively. Since Li atoms are mobile there is disorder in the system, with some of the Li atoms replacing the Cu atoms, as found experimentally. This is mimicked by considering a $1 \times 16 \times 1$ supercell resulting in 32 Cu sites in the cell, out of which some of the Cu and Li positions are interchanged, amounting to 6.25% disorder. Starting from such a structure, to derive the underlying spin model we use a muffin-tin orbital (MTO) based NMTO-downfolding calculation [36] in which effective Cu x^2-y^2 Wannier functions are constructed by integrating out all the degrees of freedom other than Cu x^2-y^2, defining a low-energy Hamiltonian. The real-space representation of the low-energy Hamiltonian shows interlayer Cu-Cu interactions to be negligibly small, with two dominant intralayer Cu-Cu hoppings, t_1 and t_5, one connecting the nearest-neighbor edge-sharing Cu atoms and the other connecting Cu atoms through superexchange paths involving O-Sb-O. The effective Cu x^2-y^2 Wannier functions are shaped according to x^2-y^2 symmetry, while the tails are shaped according to integrated O p symmetries, due to the large admixture between Cu x^2-y^2 and O p [see the inset in Fig. 4(a)]. For the nearest-neighbor interaction (t_1), the O p–like tails of two neighboring Wannier functions are orthogonal to each other. For the interaction through superexchange paths involving O-Sb-O (t_5), they point toward each other (marked with an arrow) in the figure. This makes the t_5 hopping 3.5 times stronger than t_1, although the Cu-Cu distance is 2.93 Å for t_1 and 5.79 Å for t_5. The edge-shared nearest-neighbor Cu atoms are connected through Cu-O-Cu bond angles of 89° and 86°, which gives rise to the possibility of ferromagnetic exchanges in the system. Total energy calculations in a plane-wave basis [37,38] of different magnetic configurations of Cu spins, and subsequent mapping to the Heisenberg model, show the edge-shared nearest-neighbor Cu-Cu magnetic interaction J_1 corresponding to hopping interaction t_1 to be ferromagnetic with a value -21 meV, while the long-ranged Cu-Cu magnetic interaction J_2 through Sb, corresponding to hopping interaction t_5, is shown to be antiferromagnetic with a value 31 meV. The obtained J values have been cross-checked by considering different magnetic configurations, which is found to cause very insignificant variation of only 4–5 % in the J values. Our *ab initio* results thus predict an $S = 1/2$ FM-AFM alternating chain model with $J_{AFM} \geqslant J_{FM}$, in contrast to conclusions drawn in the previous work based on fitting of susceptibility data, suggesting $J_{AFM} \leqslant J_{FM}$ [21].

Based on first-principles input, we next consider a system of fragmented FM-AFM ($J_{FM} = -21$ meV and

$J_{\mathrm{AFM}} = 31$ meV) $S = 1/2$ chains with 200 sites and random disorder ≈6.25%, given by the Hamiltonian $\mathcal{H} = \sum_i^{N/2}[J_{\mathrm{AFM}} S_{2i-1} S_{2i} + J_{\mathrm{FM}} S_{2i} S_{2i+1}] - h\sum_i^N S_i^z$, where i denotes sites occupied by Cu atoms, and h is an applied magnetic field, which was taken to be zero in our calculation. The impurity sites are chosen randomly. They host nonmagnetic Li atoms, which are obtained by replacing Cu atoms of the pristine compound. The obtained results are averaged over 50 random configurations. In a stochastic series expansion implementation of quantum Monte Carlo (SSE-QMC) [39,40], we measure the spin susceptibility as $\chi_{\mathrm{th}} = \beta J\langle S_z^2 - \langle S_z\rangle^2\rangle$, where $\beta = 1/k_B T$, which can be related to the experimentally measured molar susceptibility as $0.375\, S(S+1) g^2 \frac{\chi_{\mathrm{th}}}{T_J}$, where T_J is the temperature corresponding to dominant magnetic exchange J_{AFM}. A comparison between the calculated and measured susceptibility is shown in Fig. 4(a). Good matching between the two justifies the goodness of the *ab initio* derived spin model.

Following the successful description of the experimentally measured susceptibility results, we attempt to calculate the inelastic neutron scattering response, which measures the magnonic excitations in a quantum spin system. Theoretically, the INS amplitude can be obtained from a calculation of the frequency- and momentum-dependent dynamical structure factors [41] given by $A^l(Q,\omega) = \sum_n |\langle\psi_n|S_Q^l|\psi_0\rangle|^2 \delta(\omega - (E_n - E_0)) = -\frac{\mathrm{Im}[G(Q,\omega)]}{\pi}$. Here $l \sim x, y, z$, $|\psi_n\rangle$ is the nth eigenvector of the Hamiltonian having energy eigenvalue E_n. Our structure factor calculation is based on the 1D spin model adopted for the present system, and hence the calculated Q here is one-dimensional. It acts along the spin chain direction, which is the crystallographic b-axis for $Li_3Cu_2SbO_6$ as shown in Fig. 1(c). $G(Q,\omega)$ denotes the dynamical correlation function or Green's function, which can be written (for $l = z$) in terms of continued fraction [42] as $G(Q,\omega) = \cfrac{\langle\psi_0|S_Q^{z\dagger} S_Q^z|\psi_0\rangle}{\omega + i\eta - a_0 - \cfrac{b_1^2}{\omega + i\eta - a_1 - \cfrac{b_2^2}{\omega + i\eta - \cdots}}}$, where S_Q^z is the Fourier transform of spin-z operator S_r^z and is given by $S_Q^z = \frac{1}{\sqrt{N}}\sum_r \exp[iQ\cdot r] S_r^z$. The continued fraction can be solved iteratively first by defining $|f_0\rangle = S_Q^z|\psi_0\rangle$ and obtaining the orthogonal states, $|f_{n+1}\rangle = (\mathcal{H} - a_n)|f_n\rangle - b_n^2|f_{n-1}\rangle$, with $a_n = \langle f_n|\mathcal{H}|f_n\rangle/\langle f_n|f_n\rangle$, $b_{n+1}^2 = \langle f_{n+1}|f_{n+1}\rangle/\langle f_n|f_n\rangle$, and $b_0 = 0$. The result obtained by averaging over results from 50 random configurations is shown in Fig. 4(b). The overall features agree well with measured INS data. In particular, large structure factor values are obtained around an energy ≈8–10 meV, as also seen in experimental data at 7 K. Similar to the INS result, the calculated spectrum shows a low-energy peak near $Q = 0$, which indicates almost parallel preferential spin orientations among the nearest-neighbor $S = 1/2$ Cu^{2+} ions. This causes a FM-like behavior even though the strongest interaction is antiferromagnetic. Due to the vacancy created in the spin-lattice as a result of the random replacement of the $S = 1/2$ Cu^{2+} ions by nonmagnetic Li, an overall nonmagnetic spectral behavior dominates.

VII. SUMMARY

The important finding is that $Li_3Cu_2SbO_6$ does not order magnetically down to 50 mK even though the system has a significant value of next-nearest-neighbor (NNN) AFM exchange interaction of $J_{\mathrm{AFM}} = 31$ meV, compared to NN FM $J_{\mathrm{FM}} = -21$ meV, confirmed through our bulk as well as microscopic measurements. The plateaulike behavior in $\lambda_{\mathrm{ZF}}(T)$ and $\lambda_{\mathrm{LF}}(H)$ might indicate the development of a disordered state at low temperature due to the competing exchange interactions of J_{FM} and J_{AFM} arising from nearest neighbors and next-nearest neighbors. Finding real QSL materials is a rare phenomenon as there have been only a few candidates reported so far, such as in a pyrochlore lattice, a kagome lattice, and organic charge-transfer salts with frustrated triangular geometry, etc. Honeycomb $3d$ layered oxides with a d^9 or d^7 quasi-two-dimensional lattice $A_3A'_2BO_6$ (A = Li, Na; A' = Co, Ni; B = Sb, Te) could be potential candidates of a spin-liquid-like state as there are numbers of materials with various stacking orders of the honeycomb slabs that are seen, but these systems have not been studied yet in detail.

All data presented in this work are publicly available [43].

ACKNOWLEDGMENTS

We are grateful to Bella Lake for an interesting discussion. We would like to acknowledge financial support from the Department of Science and Technology, India (SR/NM/Z-07/2015) for the financial support, and Jawaharlal Nehru Centre for Advanced Scientific Research (JNCASR) for managing the project. A.B. would like to acknowledge the Department of Science and Technology (DST) India for Inspire Faculty Research Grant (DST/INSPIRE/04/2015/000169), and the UK-India Newton grant for funding support. T.K.B. would like to thank the Department of Science and Technology (DST), Government of India, for providing financial assistance in the form of a DST-INSPIRE fellowship (IF160418). D.T.A. would like to thank the Royal Society of London for the UK-China Newton funding, and the Japan Society for the Promotion of Science for an invitation fellowship. S.K. acknowledges the Institute of Physics for providing the computational facility, and DST-SERB, Government of India for financial assistance (SRG/2019/002143). A.M.S. thanks the SA-NRF (93549) and the UJ URC/FRC for generous financial assistance. T.S.D. acknowledges J.C.Bose Fellowship (Grant No. JCB/2020/000004) for research support.

[1] W. Li, E. M. Erickson, and A. Manthiram, Nat. Energy **5**, 26 (2020).
[2] L. Savary and L. Balents, Rep. Prog. Phys. **80**, 016502 (2016).
[3] Y. Zhou, K. Kanoda, and T.-K. Ng, Rev. Mod. Phys. **89**, 025003 (2017).
[4] A. Banerjee, C. Bridges, J.-Q. Yan, A. Aczel, L. Li, M. Stone, G. Granroth, M. Lumsden, Y. Yiu, J. Knolle *et al.*, Nat. Mater. **15**, 733 (2016).
[5] L. Balents, Nature **464**, 199 (2010).
[6] S. Yan, D. A. Huse, and S. R. White, Science **332**, 1173 (2011).

[7] J. S. Helton, K. Matan, M. P. Shores, E. A. Nytko, B. M. Bartlett, Y. Yoshida, Y. Takano, A. Suslov, Y. Qiu, J.-H. Chung, D. G. Nocera, and Y. S. Lee, Phys. Rev. Lett. **98**, 107204 (2007).

[8] S. Yamashita, Y. Nakazawa, M. Oguni, Y. Oshima, H. Nojiri, Y. Shimizu, K. Miyagawa, and K. Kanoda, Nat. Phys. **4**, 459 (2008).

[9] S. Yamashita, T. Yamamoto, Y. Nakazawa, M. Tamura, and R. Kato, Nat. Commun. **2**, 275 (2011).

[10] P. Mendels and F. Bert, J. Phys. Soc. Jpn. **79**, 011001 (2010).

[11] A. C. Shockley, F. Bert, J.-C. Orain, Y. Okamoto, and P. Mendels, Phys. Rev. Lett. **115**, 047201 (2015).

[12] S. Hwan Chun, J.-W. Kim, J. Kim, H. Zheng, C. Stoumpos, C. D. Malliakas, J. F. Mitchell, K. Mehlawat, Y. Singh, Y. Choi, T. Gog, A. Al-Zein, M. Sala, M. Krisch, J. Chaloupka, G. Jackeli, G. Khaliullin, and B. J. Kim, Nat. Phys. **11**, 462 (2015).

[13] V. M. Katukuri, R. Yadav, L. Hozoi, S. Nishimoto, and J. van den Brink, Sci. Rep. **6**, 29585 (2016).

[14] K. Kitagawa, T. Takayama, Y. Matsumoto, A. Kato, R. Takano, Y. Kishimoto, S. Bette, R. Dinnebier, G. Jackeli, and H. Takagi, Nature **554**, 341 (2018).

[15] F. Bahrami, W. Lafargue-Dit-Hauret, O. I. Lebedev, R. Movshovich, H.-Y. Yang, D. Broido, X. Rocquefelte, and F. Tafti, Phys. Rev. Lett. **123**, 237203 (2019).

[16] H. Takagi, T. Takayama, G. Jackeli, G. Khaliullin, and S. E. Nagler, Nat. Rev. Phys. **1**, 264 (2019).

[17] C. Wong, M. Avdeev, and C. D. Ling, J. Solid State Chem. **243**, 18 (2016).

[18] L. C. Wang, X. P. Li, and C. F. Li, Phys. Rev. B **95**, 104308 (2017).

[19] A. I. Kurbakov, A. N. Korshunov, S. Y. Podchezertsev, A. L. Malyshev, M. A. Evstigneeva, F. Damay, J. Park, C. Koo, R. Klingeler, E. A. Zvereva, and V. B. Nalbandyan, Phys. Rev. B **96**, 024417 (2017).

[20] A. Scheie, K. Ross, P. P. Stavropoulos, E. Seibel, J. A. Rodriguez-Rivera, J. A. Tang, Y. Li, H.-Y. Kee, R. J. Cava, and C. Broholm, Phys. Rev. B **100**, 214421 (2019).

[21] C. Koo, E. A. Zvereva, I. L. Shukaev, M. Richter, M. I. Stratan, A. N. Vasiliev, V. B. Nalbandyan, and R. Klingeler, J. Phys. Soc. Jpn. **85**, 084702 (2016).

[22] Y. Miura, Y. Yasui, T. Moyoshi, M. Sato, and K. Kakurai, J. Phys. Soc. Jpn. **77**, 104709 (2008).

[23] See Supplemental Material at http://link.aps.org/supplemental/10.1103/PhysRevB.103.174423 for experimental details, Neutron diffraction, heat capacity, Neutron Scattering, Spin Wave Simulation.

[24] V. Kumar, A. Gupta, and S. Uma, Dalton Trans. **42**, 14992 (2013).

[25] M. I. Stratan, I. L. Shukaev, T. M. Vasilchikova, A. N. Vasiliev, A. N. Korshunov, A. I. Kurbakov, V. B. Nalbandyan, and E. A. Zvereva, New J. Chem. **43**, 13545 (2019).

[26] M. Fujihala, K. Morita, R. Mole, S. Mitsuda, T. Tohyama, S.-i. Yano, D. Yu, S. Sota, T. Kuwai, A. Koda, H. Okabe, H. Lee, S. Itoh, T. Hawai, T. Masuda, H. Sagayama, A. Matsuo, K. Kindo, S. Ohira-Kawamura, and K. Nakajima, Nat. Commun. **11**, 3429 (2020).

[27] A. Fukaya, I. Watanabe, S. Ohira, and K. Nagamine, Phys. B **289–290**, 185 (2000).

[28] Y. J. Uemura, A. Keren, K. Kojima, L. P. Le, G. M. Luke, W. D. Wu, Y. Ajiro, T. Asano, Y. Kuriyama, M. Mekata, H. Kikuchi, and K. Kakurai, Phys. Rev. Lett. **73**, 3306 (1994).

[29] O. Mustonen, S. Vasala, E. Sadrollahi, K. P. Schmidt, C. Baines, H. C. Walker, I. Terasaki, F. J. Litterst, E. Baggio-Saitovitch, and M. Karppinen, Nat. Commun. **9**, 1085 (2018).

[30] M. Gomilšek, M. Klanjšek, M. Pregelj, F. C. Coomer, H. Luetkens, O. Zaharko, T. Fennell, Y. Li, Q. M. Zhang, and A. Zorko, Phys. Rev. B **93**, 060405(R) (2016).

[31] A. Zorko, F. Bert, P. Mendels, P. Bordet, P. Lejay, and J. Robert, Phys. Rev. Lett. **100**, 147201 (2008).

[32] R. Sarkar, P. Schlender, V. Grinenko, E. Haeussler, P. J. Baker, T. Doert, and H.-H. Klauss, Phys. Rev. B **100**, 241116(R) (2019).

[33] B. Gao, T. Chen, D. W. Tam, C.-L. Huang, K. Sasmal, D. T. Adroja, F. Ye, H. Cao, G. Sala, M. B. Stone, C. Baines, J. A. T. Verezhak, H. Hu, J.-H. Chung, X. Xu, S.-W. Cheong, M. Nallaiyan, S. Spagna, M. B. Maple, A. H. Nevidomskyy, E. Morosan, G. Chen, and P. Dai, Nat. Phys. **15**, 1052 (2019).

[34] O. A. Petrenko, O. Young, D. Brunt, G. Balakrishnan, P. Manuel, D. D. Khalyavin, and C. Ritter, Phys. Rev. B **95**, 104442 (2017).

[35] W. Kohn and L. J. Sham, Phys. Rev. **140**, A1133 (1965).

[36] O. K. Andersen and T. Saha-Dasgupta, Phys. Rev. B **62**, R16219 (2000).

[37] G. Kresse and J. Hafner, Phys. Rev. B **47**, 558 (1993).

[38] G. Kresse and J. Furthmüller, Phys. Rev. B **54**, 11169 (1996).

[39] A. W. Sandvik, Phys. Rev. B **59**, R14157 (1999).

[40] A. Dorneich and M. Troyer, Phys. Rev. E **64**, 066701 (2001).

[41] A. Klauser, J. Mossel, J.-S. Caux, and J. van den Brink, Phys. Rev. Lett. **106**, 157205 (2011).

[42] E. R. Gagliano and C. A. Balseiro, Phys. Rev. Lett. **59**, 2999 (1987).

[43] T. Sinha *et al.*, Muon spin relaxation study of Halden like spin chains in Layered $Li_3Cu_2SbO_6$, STFC ISIS Neutron and Muon Source, https://doi.org/10.5286/ISIS.E.RB1968007